Invertebrate Zoology, 2025, 22(4): 575–594

Localization and distribution dynamics of total maternal RNA in oocytes and early embryos of *Platynereis dumerilii* (Annelida)

R.I. Mullakhmetov[1], E.A. Kondakova[2,3], G.P. Maslakov[2,4], L.O. Poliushkevich[2], M.A. Kulakova[2*]

[1] *Department of Cytology and Histology, St. Petersburg State University, Universitetskaya Emb., 7/9, St. Petersburg 199034 Russia.*
[2] *Department of Embryology, St. Petersburg State University, Universitetskaya Emb., 7/9, St. Petersburg 199034 Russia.*
[3] *Saint Petersburg Branch of the FSBSI "VNIRO" ("GosNIORKH" named after L.S. Berg), Makarova Emb., 26, St. Petersburg 199053 Russia.*
[4] *Laboratory of Regenerative Biomedicine, Institute of Cytology, Russian Academy of Sciences, Tikhoretskiy Prospekt, 4, St Petersburg 194064 Russia.*
** Corresponding author: m.kulakowa@spbu.ru*
Roman Mullakhmetov: mullakhmetov.03@mail.ru ORCID https://orcid.org/0009-0007-0700-971X
Ekaterina Kondakova st036262@mail.spbu.ru ORCID https://orcid.org/0000-0002-5117-4858
Georgii Maslakov: ORCID gequris@gmail.com https://orcid.org/0000-0003-0462-7284
Liudmila Poliushkevich: mila.papurika@gmail.com ORCID https://orcid.org/0000-0003-2896-1893
Milana Kulakova: m.kulakowa@spbu.ru ORCID https://orcid.org/0000-0001-9814-3875

ABSTRACT: The early developmental events of all multicellular animals are governed by the maternal genome. Maternal RNA plays a crucial role in sustaining the viability and growth of the early embryo, providing molecular instructions for each initial cell division and facilitating the transition to embryonic development under zygotic genome control. Consequently, the fate of each blastomere depends on its unique set of maternal determinants, which may be critically important for the successful progression of stereotypical and invariant cleavage patterns observed in spiralians. How is maternal RNA distributed in the embryo of a typical spiralian representative? What is its quantity, and for how long is it preserved? The laboratory annelid *Platynereis dumerilii* is an excellent model to address these questions, as it exhibits a highly stereotypical pattern of spiral cleavage and contains at least 4,000 maternally contributed transcripts. However, current transcriptomic approaches have not provided insights into the distribution of maternal RNA among individual blastomeres of *P. dumerilii*, and single-cell sequencing has yet to be applied to the early developmental stages of this species. To address this critical gap, we quantified the average amount of maternal RNA for a single oocyte and, for the first time, visually characterized its segregation in early *P. dumerilii* embryos up to the 16-cell stage, prior to zygotic genome activation. Our findings reveal that maternal RNA in *P. dumerilii* is initially distributed around the oocyte nucleus and rapidly relocates to the animal pole following fertilization. Its subsequent segregation closely aligns with unequal-cleavage dynamics. One cell cycle prior to the first wave of zygotic transcription, nearly all maternal RNA concentrates in the first quartet of micromeres $1a^1$-$1d^1$ and the first somatoblast 2d. Notably, these localization dynamics diverge from observations in another annelid, *Chaetopterus.* Our findings offer a foundation for future comparative and experimental studies on how maternal components regulate early development in spiralians.
How to cite this article: Mullakhmetov R.I., Kondakova E.A., Maslakov G.P., Poliushkevich L.O., Kulakova M.A. 2025. Localization and distribution dynamics of total maternal RNA in oocytes and early embryos of *Platynereis dumerilii* (Annelida) // Invert. Zool. Vol.22. No.4. P.575–594, Suppl. files. doi: 10.15298/invertzool.22.4.05

KEY WORDS: Maternal RNA, oocytes, spiral cleavage, RNA segregation, *Platynereis,* annelids, nuclear F-actin.

Локализация и динамика распределения суммарной материнской РНК в ооцитах и ранних эмбрионах *Platynereis dumerilii* (Annelida)

Р.И. Муллахметов[1], Е.А. Кондакова[2,3], Г.П. Маслаков[2,4], Л.О. Полюшкевич[2], М.А. Кулакова[2*]

[1] *Кафедра цитологии и гистологии, Биологический факультет, Санкт-Петербургский государственный университет, Университетская наб., 7–9, Санкт-Петербург 199034 Россия.*
[2] *Кафедра эмбриологии, Биологический факультет, Санкт-Петербургский государственный университет, Университетская наб., 7–9, Санкт-Петербург 199034 Россия.*
[3] *Санкт-Петербургский филиал ФГБНУ «ВНИРО» («ГосНИОРХ» им. Л.С. Берга), набережная Макарова, д.26, Санкт-Петербург 199053 Россия.*
[4] *Лаборатория Регенеративной Биомедицины, Институт цитологии РАН, Тихорецкий просп. 4, Санкт-Петербург 194064 Россия.*
** Corresponding author: m.kulakowa@spbu.ru*

РЕЗЮМЕ: Раннее развитие всех многоклеточных животных регулируются материнским геномом. Материнская РНК критически важна для жизнеспособности и роста раннего эмбриона. Она предоставляет молекулярные инструкции для первых делений дробления и облегчает переход под контроль зиготического генома. При стереотипных и инвариантных моделях дробления судьба каждого бластомера особенно тесно связана с уникальным набором материнских детерминант. Как распределяется материнская РНК в эмбрионе спиральных животных? Сколько её и как долго она сохраняется? Аннелида *Platynereis dumerilii* — превосходная модель для решения этих вопросов. *P. dumerilii* демонстрирует высоко стереотипную модель спирального дробления и содержит не менее 4000 транскриптов, внесенных матерью. Однако современные транскриптомные подходы не дали представления о распределении материнской РНК среди отдельных бластомеров *P. dumerilii*, а секвенирование отдельных клеток еще не применялось к ранним стадиям развития этого вида. Чтобы частично устранить этот критический пробел, мы определили среднее количество материнской РНК в одном ооците и впервые визуально охарактеризовали ее сегрегацию в ранних эмбрионах *P. dumerilii* вплоть до 16-клеточной стадии, т.е. до активации зиготического генома. Наши результаты показывают, что материнская РНК в *P. dumerilii* изначально распределена вокруг ядра ооцита и быстро перемещается к анимальному полюсу после оплодотворения. Ее последующая сегрегация тесно связана с динамикой неравного дробления. Выяснилось, что за один клеточный цикл до первой волны зиготической транскрипции почти вся материнская РНК концентрируется в первом квартете микромеров 1a^1-1d^1 и первом соматобласте 2d. Примечательно, что динамика локализации РНК расходится с наблюдаемой у другого кольчатого червя, *Chaetopterus*. Наши результаты предлагают основу для будущих сравнительных и экспериментальных исследований того, как материнские компоненты регулируют раннее развитие у спиральных животных.

Как цитировать эту статью: How to cite this article: Mullakhmetov R.I., Kondakova E.A., Maslakov G.P., Poliushkevich L.O., Kulakova M.A. 2025. Localization and distribution dynamics of total maternal RNA in oocytes and early embryos of *Platynereis dumerilii* (Annelida) // Invert. Zool. Vol.22. No.4. P.575–594, Suppl. files. doi: 10.15298/invertzool.22.4.05

КЛЮЧЕВЫЕ СЛОВА: материнские РНК, ооциты, спиральное дробление, распределение РНК, *Platynereis,* аннелиды, ядерный F-актин.

Introduction

Early embryonic development in metazoans relies on RNA and proteins synthesized from the maternal genome. In most animals, cleavage occurs before the zygotic genome activation and it relies entirely on resources stored in the oocyte. For instance, in amphibians, an enucleated egg can develop up to the blastula stage (Briggs *et al.*, 1951), solely using maternal contributions. In multicellular animals, these contributions are represented by structural and regulatory proteins and their mRNAs, which are either non-uniformly distributed in the oocyte or become differentially localized shortly after fertilization. In most cases, the segregation of these maternal determinants shapes the embryo's developmental architecture, by establishing geometric axes and specifying cell lineages.

The maternal genome handles complex and often conflicting tasks. One of its primary functions is to suppress premature zygotic genome activation, as transcription and replication are mutually incompatible processes. Second, it must supply the dividing embryo with building blocks in the form of macromolecular precursors, functional tools in the form of housekeeping RNA and proteins, and a set of molecular instructions that direct early development. Third, maternal determinants must activate the zygotic genome following the rapid cleavage phase and coordinate its function, including regulating dosage compensation between maternal and paternal alleles. This transfer of developmental control is known as the maternal-to-zygotic transition (MZT). A fourth critical task is the timely elimination of maternal RNAs and proteins by the time of the MZT. These roles are carried out by a diverse array of macromolecules, with maternal RNAs being particularly significant. Oocytes are known to contain several times more unique RNAs synthesized from single-copy DNA loci than any differentiated cells in the body (Davidson, Britten, 1979; Davidson, 1986), yet the functions of most of these unique maternal RNAs remain largely unexplored, even in model organisms.

Spiralians provide an ideal system to study the distribution of maternal determinants and their influence on the fate of descendant cells, due to their invariant and stereotypical blastomere divisions. Early investigations in the annelid *Chaetopterus* examined the localization of specific maternal RNA populations, including ribosomal, histone, and total polyadenylated RNAs (Jeffery, Wilson, 1983). It was found that these RNAs preferentially associate with both the animal and vegetal cortices, resulting in an orderly distribution during cleavage. A possible mechanism underlying such non-random distribution was described in the mollusk *Ilyanassa*, where *Dpp* and *Eve* transcripts bind to one centrosome of the pair, then associate with the cortex, and become asymmetrically inherited by blastomeres (Lambert, Nagy, 2002). Furthermore, the establishment of asymmetric cleavage itself is regulated by maternal factors (Nakama *et al.*, 2017). Subsequently, maternal contributions to early development in model mollusks and annelids have been investigated using 'omics' technologies (Liu *et al.*, 2014; Chou *et al.*, 2016).

Introducing new model organisms in developmental biology often leads to significant discoveries. In this context, the annelid *Platynereis dumerilii* has emerged as an outstanding model for investigating the structural and functional evolution of genes involved in morphogenesis (Özpolat *et al.*, 2021). A comprehensive transcriptome analysis of *P. dumerilii* zygotes and early embryos revealed the dynamics of 28,580 genes, approximately 4000 of which are maternally transcribed (Chou *et al.*, 2016). This study demonstrated that the first waves of zygotic gene expression in the worm embryo begin at the ~30 cell stage (6 hours post-fertilization; hpf). The final step of the MZT occurs relatively late, between 8 and 10 hpf. By this stage, the embryo already consists of 66–140 cells and its cleavage pattern becomes bilaterally symmetric (Chou *et al.*, 2016).

In *P. dumerilii*, each blastomere gives rise to progeny with a defined fate—a process that, in its earliest stages, depends critically on the segregation of maternal determinants. Although transcriptomic approaches have expanded our understanding of overall gene expression, they do not provide insights into the distribution of maternal RNA among individual blastomeres, and single-cell sequencing has yet to be applied to the early developmental stages of this annelid. To address this gap, we investigated the segregation of maternal RNA using conventional methods. In this study, we quantified the total RNA content per *P. dumerilii* oocyte and mapped its localization up to the 16-cell stage (5 hpf) using fluorescent

imaging techniques, prior to the onset of zygotic expression for the majority of genes.

Material and methods

P. dumerilii culture, sampling, and fixation

The laboratory culture of *P. dumerilii* was maintained at 18 °C in artificial seawater (Red Sea Salt dissolved in distilled water) with a salinity of 32‰, under artificial lighting conditions designed to simulate a lunar cycle (Fischer, Dorresteijn, 2004). Animals were fed twice, weekly, with homogenized spinach and a mixture of ground seafood (shrimp, mussels, squid; volumetric ratio 2:1:0.5). Mature males and females were housed in separate containers.

For RNA extraction and staining experiments, we collected naturally spawned oocytes. In previous trials, eggs obtained through female dissection showed significantly lower fertilization rates, likely due to compromised integrity (data not shown). Therefore, to accurately examine the concentration and distribution of total RNA in oocytes, it was necessary to use naturally released eggs. In *P. dumerilii*, reproductive behavior is synchronized by sex-specific pheromones (Hardege *et al.*, 1998; Röhl *et al.*, 1999). To induce spawning, we exposed mature females to seawater containing male-produced pheromones. Two females were transferred to a glass tray (700 mL) with 350 mL seawater, while a mature male was placed in a 60 mL syringe filled with 10 mL seawater and a 0.22 µm filter to retain sperm (spherical head sperm ~2.6 µm length × 1.8 µm diameter; cit. ex Valvassori, 2018). Gentle pressure applied to the male's body released pheromones into the syringe water, which was then dispensed dropwise onto females until spawning occurred (~5 mL total). Oocytes were collected post-spawning for RNA extraction or fixation.

To obtain early embryos, two mature females and one male were transferred to a separate glass tray and allowed to spawn. Fertilized oocytes were then incubated at 18°C until they reached the desired developmental stage and were sequentially fixed.

Collected oocytes and embryos were fixed overnight at 4°C in 4% paraformaldehyde (PFA). After fixation, samples were washed with phosphate-buffered saline containing 0.2% Tween-20 (PBS-T, pH 7.4), dehydrated through a graded methanol series, and stored in 100% methanol at –20 °C overnight or longer. A portion of the samples was immediately stained after PBS-T washing, as detailed in the Staining section below.

Extraction and quantification of total RNA from *P. dumerilii* oocytes

Efficient extraction of maternal RNA from *P. dumerilii* oocytes is complicated by their high polysaccharide content, which increases solution viscosity, precipitates with RNA, reduces yield, interferes with quantification, and inhibits downstream applications (Ghawana *et al.*, 2011). To mitigate these issues, we adapted an RNA extraction method originally used for plants (Kiss *et al.*, 2024), employing cetyltrimethylammonium bromide (CTAB), a strongly cationic surfactant. This protocol includes an initial nucleic acid extraction step, followed by phase separation using phenol-chloroform, and a final precipitation step (File S1). CTAB serves as a strong detergent, disrupting cellular membranes and facilitating the separation of nucleic acids from polysaccharides under high-salt conditions. During phenol-chloroform phase separation, polysaccharides predominantly partition into the interphase, leaving RNA enriched in the aqueous supernatant (Wang, Stegemann, 2010). Following extraction, RNA concentrations were determined using a Bio-Rad SmartSpec Plus Spectrophotometer (Bio-Rad, USA) in "RNA" measurement mode. RNA integrity was assessed by agarose gel electrophoresis (Fig. S1).

To estimate RNA content per oocyte, we quantified oocytes within a 100 µL aliquot taken from 1 mL of thoroughly mixed oocytes. Automated counting was performed using machine learning algorithms via the DLgram cloud service (Matveev *et al.*, 2024). An example of microscopy image with oocytes labeled by the algorithm is provided in Fig. S2. Oocytes not detected by the algorithm were manually counted using Fiji software (Schindelin *et al.*, 2012). The RNA content per oocyte was calculated as:

. The standard error of the mean was calculated using the std.error() function from the plotrix library in R Studio (Lemon, 2006). Total RNA quantification was performed using pooled oocytes from three biological replicates, with each replicate consisting of eggs from two sexually mature, medium-sized females.

Histology and bright-field microscopy

The methanol stored samples were embedded into paraffin, (Paraplast, Leica) according to the standard procedure. Paraffin sections, 5–6 µm thick, were cut using a Leica SM-2010R sleigh microtome (Leica Microsystems, Germany). The sections were stained with Carazzi's hematoxylin and eosin (Biovitrum, Russia) and mounted in Vitrogel (Biovitrum, Russia). Imaging and photography were performed using a Leica DMI6000 microscope (Leica Microsystems, Germany) equipped with a Leica DFC495 CCD digital camera (Leica Microsystems, Germany). Photographs were processed using Adobe Photoshop CS 5.1. (Adobe Photoshop, RRID: SCR_014199).

Staining with fluorescent dyes, immunocytochemistry, and confocal laser scanning microscopy

For fluorescent staining, the following dyes were used: carbocyanine fluorescent dye TO-PRO1 iodide (Ex/Em: 515/531 nm) for RNA, Hoechst 33342 (Ex/Em: 350/461 nm) and Methyl green (Ex/Em: 633/677

nm upon DNA binding) for DNA, Phalloidin-TRITC (Ex/Em: 544/570 nm) for F-actin. Prior to staining, samples were washed with PBS-T to remove the fixative and blocked for 1 hour at room temperature in Blocking Reagent (Roche, Switzerland). The samples were then incubated overnight at 4°C with primary anti-acetylated tubulin antibody (mouse monoclonal; Sigma) (1:300). After washing with PBS-T, the samples were stained with TO-PRO1 (0.1 mM; 1:800), Hoechst 33342 (1 μg/μL; 1:800), Phalloidin-TRITC (100 ng/μL; 1:40), and secondary antibodies (anti-mouse CF633, Ex/Em: 633/635 nm; 1:300). Staining was performed overnight at 4 °C. In addition, control samples for autofluorescence in the TO-PRO1 channel were prepared by staining oocytes and early-stage embryos with Phalloidin-TRITC and Methyl Green. Following staining, the samples were washed with PBS-T, mounted in Mowiol medium, and allowed to solidify for 24 hours. A portion of the material was mounted in 100% glycerol and scanned on the day of washing.

Imaging and quantification of RNA fluorescence

Imaging was carried out using a Leica TCS SP5 Confocal Laser Scanning Microscope (Leica Microsystems, Germany), equipped with a TrueChrome 4K Pro digital camera. Image processing and analysis were performed using Bitplane Imaris 7.7.0 (Imaris, RRID:SCR_007370).

To describe the distribution of RNA in different blastomeres, we conducted fluorescence intensity measurements of the TO-PRO1 channel in blastomeres from three embryos for each of the 4-, 8-, and 16-cell stages. For this, we used the 3D Objects Counter plugin in Fiji, which enabled us to calculate the volume (in microns and voxels) and the integrated density for each blastomere (Bolte, Cordelières, 2006; Schindelin *et al.*, 2012). Integrated density is defined as the sum of all voxel values within our region of interest (ROI). Unfortunately, the plugin was unable to recognize the blastomeres as distinct 3D objects in the Z-stacks. Therefore, we manually selected the blastomeres as ROIs and subsequently used the "Mask(s) from ROI(s)" plugin to generate ground-truth segmentation masks (Thomas, Trehin, 2021). This segmentation was performed based on data from two channels: the TO-PRO1 channel and the F-actin channel. The resulting masks were then utilized for the fluorescence intensity measurements with the 3D Objects Counter.

To compare total RNA abundance across blastomeres from three replicate embryos, we calculated the Corrected Total Cell Fluorescence (CTCF), which involves subtracting the background fluorescence from the integrated density. CTCF is defined as follows: The mean background fluorescence was measured using the same method as for the ROI. The computed values are provided in File S2. Boxplots displaying CTCF values for each blastomere were generated in R Studio. To compare the CTCF values of the $1q^1$ and $1q^2$ micromeres at the 16-cell stage, we applied the Mann–Whitney U test using the wilcox.test() function in R Studio.

Results

Quantification of RNA in single *P. dumerilii* oocytes

Nereid annelids exhibit a pronounced r-selection reproductive strategy, characterized by high reproductive output and minimal parental investment. A single *P. dumerilii* female can spawn anywhere from 400 to 16,000 oocytes, with a previously reported average of 2,000–3,000 eggs (Fischer, Dorresteijn, 2004; Metzger, Özpolat, 2024). In this study, we quantified the number of oocytes spawned by two females and determined the average total RNA content per oocyte. The results, derived from three biological

Table 1. Calculation of mean total RNA per *P. dumerilii* oocyte.

Biological replicate	Oocytes* per extraction	Total RNA (ng)	Total RNA per oocyte (ng)
1	14600	131500	9.01
2	17070	169874	9.95
3	10570	122040	11.55
Mean total RNA per oocyte (ng)		10.17±0.74	

* — oocytes were spawned by two mature females simultaneously.

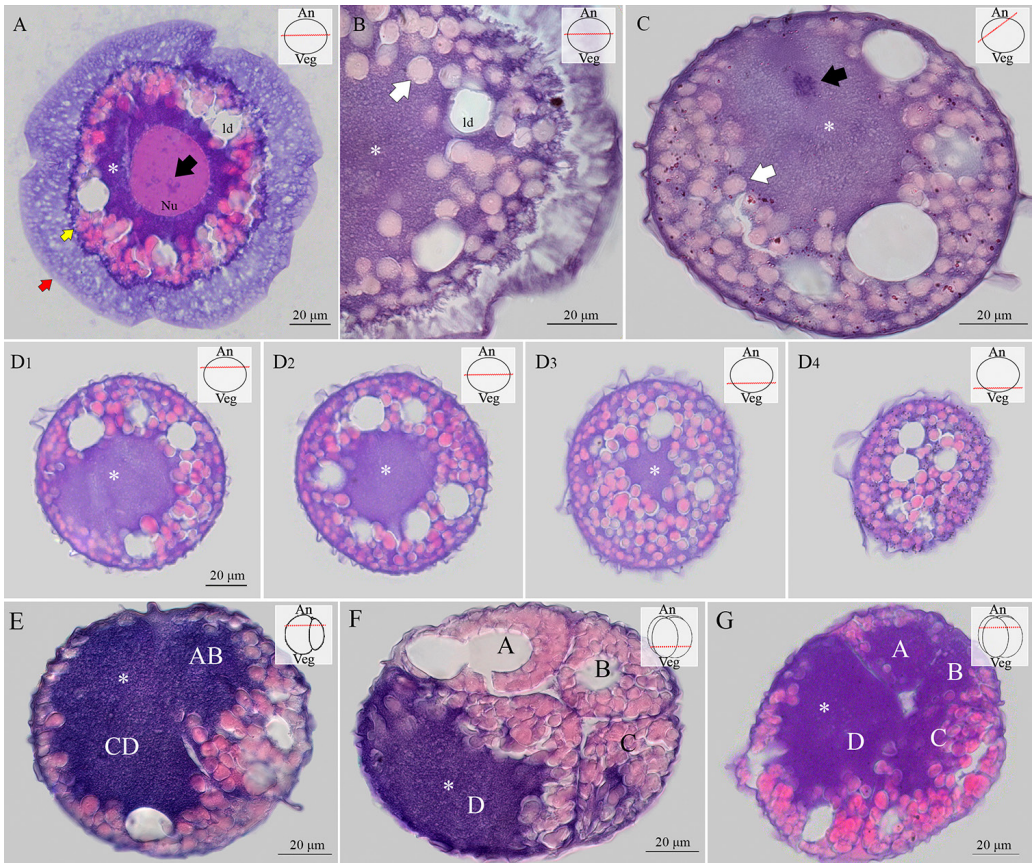

Fig.1. Histological sections of *Platynereis dumerilii* oocytes and early embryos stained with Carazzi's hematoxylin and eosin. A, B — oocyte; C, D — zygote (0.5 hpf); D1–D4 — consecutive sections selected from the complete series, arranged from animal to vegetal pole, demonstrate that basophilic material containing maternal RNA is concentrated at the animal pole of the zygote; E — 2-cell embryo, section through the animal pole of the embryo, showing significant accumulation of basophilic material (including total RNA) in the larger blastomere CD; F, G — 4-cell embryo, the yellow arrow indicates the boundary between the oocyte and the surrounding egg jelly layer (marked by the red arrow, see main text), white arrows indicate yolk protein granules, while the black arrow points to the chromosomes, the asterisk marks basophilic material containing maternal RNA.
Abbreviations: ld — lipid droplet cavities; Nu — nucleus.

replicates involving both oocyte counting and RNA extraction, are summarized in Table 1. Our findings indicate a mean total RNA content of 10.17 ng per oocyte.

Redistribution of nuclear and cytoplasmic components after fertilization

To gain a general understanding of the organization of the oocyte, zygote, and early embryos in *P. dumerilii*, we obtained serial histological sections stained with Carazzi's hematoxylin and eosin. Hematoxylin, a positively charged basic dye, binds to negatively charged (basophilic) cellular structures such as DNA and RNA, as well as ribosomes in the cytoplasm, producing a blue stain. Although hematoxylin staining is not specific to RNA alone, the observed cytoplasmic staining reflects the presence of both mRNA and rRNA, which we collectively considered part of the maternally inherited total RNA pool in this study. Eosin, a negatively charged acidic dye, binds to positively charged (eosinophilic) structures, primarily cytoplasmic proteins, producing a red-pink stain. In oocytes and early embryos

(2-cell and 4-cell stages), the nucleoplasm and proteins stored in yolk protein granules, which are localized at the cell periphery, exhibited eosinophilic staining (Fig. 1). In the oocyte, the chromatin within the nucleus, the perinuclear region and the acidic mucopolysaccharides of cortical granules are stained basophilically (Fig. 1A–B). The most intense basophilic staining was observed in the perinuclear region, suggesting a high concentration of stored maternal RNA in this area. This result is confirmed with staining with TO-PRO-1 iodide (see below). The fixation and subsequent processing of oocytes result in the release of egg jelly precursor from cortical granules (Kluge *et al.*, 1995), forming a thick layer of egg jelly (Fig. 1A). Additionally, in early embryos, the sample preparation process caused the loss of lipids, with large spherical cavities remaining in place of lipid droplets.

Thirty minutes post-fertilization (0.5 hpf), the basophilic material, including total RNA, along with the oocyte chromosomes, migrates toward the animal pole (Fig. 1C; 1D1–D4). Figure 1D1–D4 shows this displacement in consecutive sections of one representative zygote selected from the series; the complete series of sections is provided in Fig. S3. We have carefully examined the strictly serial sections of six zygotes. At 2.5 hpf, the first cleavage produces two unequal blastomeres, AB and CD. At this stage, maternal RNA and basophilic proteins accumulate at the animal poles of the both blastomeres, while eosinophilic yolk protein granules remain localized at the vegetal pole (Fig. 1E). At 3.5 hpf, the second cleavage occurs perpendicular to the first, giving rise to four blastomeres, the progenitors of the A-, B-, C - and D-cell lineages, with the largest blastomere D in contact with blastomere B. At this stage, the vegetal pole of the embryo remains predominantly filled with yolk protein granules, whereas the basophilic material is concentrated in the animal cytoplasm of each of the four blastomeres (Fig. 1F–G).

Distribution of maternal RNA

To visualize total maternal RNA in oocytes and early embryos, we used the fluorescent carbocyanine dye TO-PRO-1 iodide (Ex/Em: 515/531 nm). *P. dumerilii* oocytes and early embryos did not show autofluorescence in the emission spectrum of this dye (Fig. S4). This dye is non-fluorescent in the absence of nucleic acids and binds to both RNA and DNA. DNA was counterstained with Hoechst 33342, which, unlike DAPI, exhibits minimal affinity for RNA. This combination allows clear differentiation between RNA and DNA signals. It is important to note that TO-PRO-1 staining is not specific to mRNA but labels total RNA, including rRNA. As mentioned earlier, we consider rRNA as part of the maternal RNA pool, given that ribosomes are maternally inherited and synthesized prior to fertilization. Additionally, we used antibodies against acetylated tubulin, previously validated in *P. dumerilii* nectochaetes (Fig. S5). However, no specific signals were detected within the oocytes or early embryos. Notably, at the 0.5 hpf stage, these antibodies stained discrete spots on the oocyte surface and small, round speckles within lipid droplet cavities (Fig. S6). Starting from the 2-cell stage, some samples were stained with Phalloidin-TRITC. This staining protocol excludes storage in methanol, as alcohols disrupt actin filaments in the specimens. Since methanol also acts as an additional fixative, its absence may affect RNA preservation and/or its native localization.

OOCYTES. Total maternal RNA is concentrated around the oocyte nucleus in a dense, unstructured cloud, gradually thinning toward the periphery (Fig. 2A-B1). It forms a distinct "star-shaped" pattern within the cytoplasm, which is free of yolk protein granules and large lipid droplet cavities. Well-preserved RNA is not detected within nuclei or lipid droplet cavities. The egg jelly becomes distinctly visible due to a small amount of stained RNA exiting cells alongside polysaccharides (Fig. 2A1-B1, red arrow). We noticed that the interval between staining and scanning influences the observed RNA distribution pattern, with longer delays resulting in a more diffuse signal. Specifically, the time required for the mounting medium (Mowiol) to solidify (~24 hours) already alters the pattern, although the general "star-shaped" RNA distribution remains consistent (Fig. 2B-B1). Notably, chromosomes in these samples exhibit enhanced staining with Hoechst 33342. We hypothesized that RNA degradation might occur during the solidification period of the mounting medium. To test this hypothesis, we treated some samples with RNase A (30 min at 37°C; Fig. 2C-C1). Interestingly, this treatment had minimal impact on RNA staining intensity but

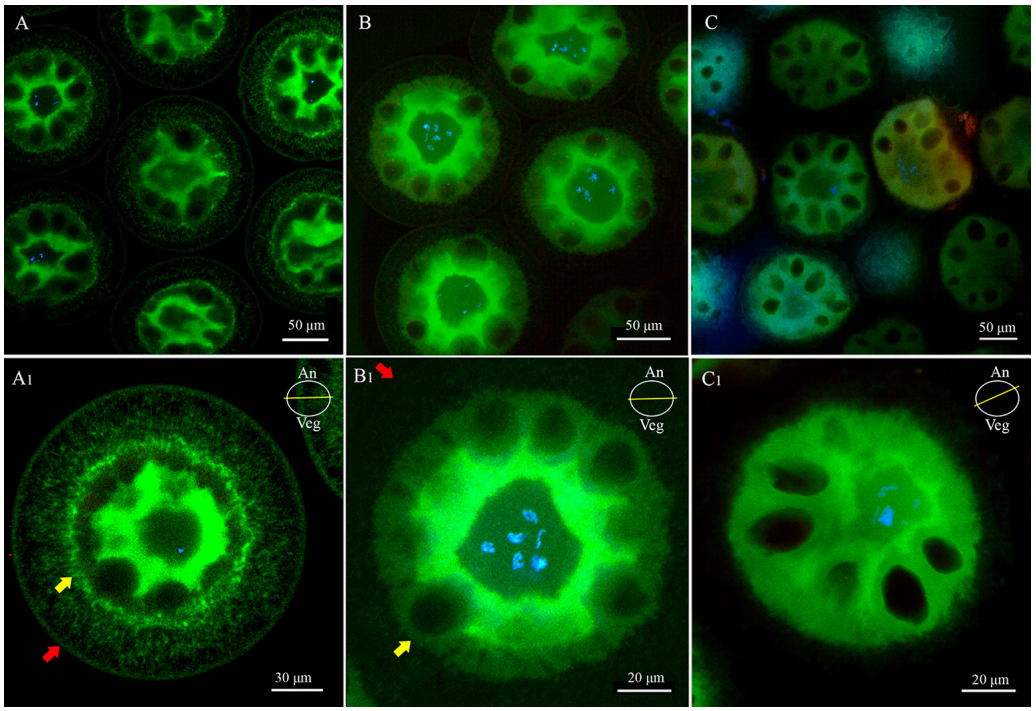

Fig. 2. Oocytes of *Platynereis dumerilii*. A, A1 — oocytes mounted in glycerol and scanned immediately after staining; B, B1 — oocytes mounted in Mowiol mounting medium, solidifying for approximately 24 hours before scanning; C, C1 — oocytes treated with RNase A. Panels with the index "1" show an enlarged view of a single oocyte, the red arrow indicates the egg jelly, while the yellow arrows denote the boundary between it and the oocyte. Staining: TO-PRO-1 iodide (RNA, green), Hoechst 33342 (DNA, blue), primary anti-acetylated tubulin antibodies (mouse monoclonal) and secondary antibodies (anti-mouse CF633) (red).

caused widespread diffusion of RNA fragments, including into the nucleus (Fig. 2C1). Following RNase A treatment, RNA diffuses extensively, and egg jelly staining disappears entirely (Fig. 2C1). For subsequent developmental stages, the egg jelly was removed by washing. Overall, the total maternal RNA in oocytes is nucleocentric and does not exhibit polar accumulation.

ONSET OF OOPLASMIC SEGREGATION (0.5 hpf). The study by Adriaan W.C. Dorresteijn (Dorresteijn, 1990) demonstrated that, at 18 °C, approximately one hour elapses between fertilization, marked by the initiation of the cortical reaction, and the entry of the sperm into the ooplasm. During the first 30 minutes of this interval, the oocyte disassembles the nuclear envelope and clears the prospective animal pole of yolk protein granules. In this region, the chromosomes (2n, 4c) become positioned, surrounded by the yolk-free cytoplasm (clear cytoplasm) that was previously located around the nucleus. The first polar body is extruded just before the sperm enters the ooplasm through a specialized cytoplasmic bridge. The second polar body is formed 19 min after the first, followed by the fusion of the pronuclei 10 min later (Dorresteijn, 1990).

In this study, several of these events are observed against the backdrop of brightly fluorescing, abundant maternal RNA. The following description is based on an examination of 13 zygotes. The RNA occupies the entire clear cytoplasm, effectively contrasting with the unstained yolk protein granules and lipid droplet cavities (Fig. 3A–C). By 0.5 hpf, the majority of the maternal RNA concentrates at the animal pole (Fig. 3D1–D4). During this period, the oocyte chromosomes form a symmetrical structure (Fig. 3B). The RNA appears as a diffuse cloud; however, in the plane of aligned chromosomes, it takes on a more structured appearance (Fig. 3B), possibly highlighting elements of the meiotic spindle.

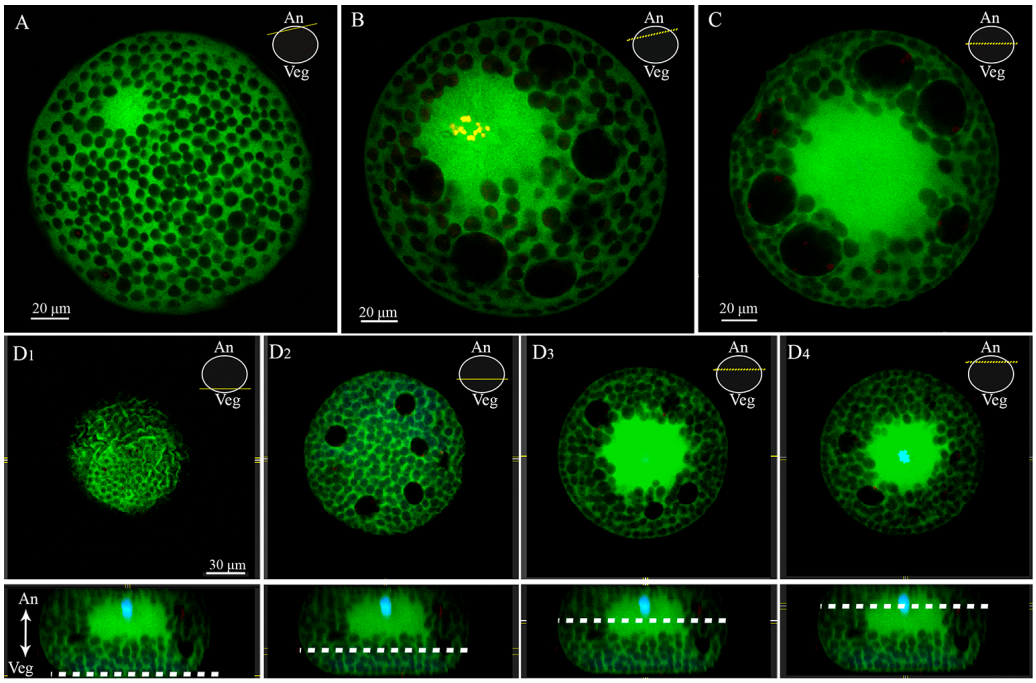

Fig. 3. Zygotes (0.5 hpf) of *Platynereis dumerilii*. A, B — the same cell, scanned near the animal pole surface (A) and closer to the equator (B), RNA (green) is concentrated near the animal pole; C — cell scanned at the equatorial level; D1–D4 — distribution of maternal RNA and yolk protein granules along the animal-vegetal axis. Positions of optical sections are indicated by white dashed lines. Staining: TO-PRO-1 (RNA, green), Hoechst 33342 (DNA, yellow, blue).

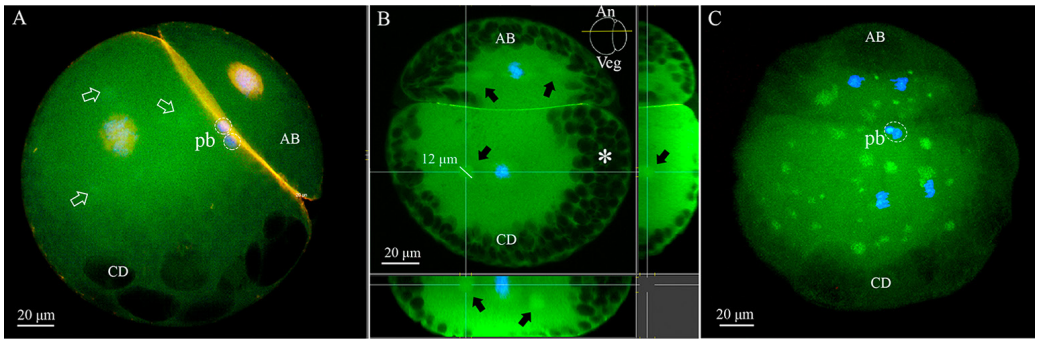

Fig. 4. Two-cell embryo at different stages of the cell cycle of *Platynereis dumerilii*. A— embryo in the post-mitotic G1 phase, the hallmark of this brief stage is the presence of F-actin in the nucleus (orange), hollow arrows point to RNA clusters similar to those in C; B — pre-mitotic embryo with a broad expanse of yolk-free cytoplasm (labeled with maternal RNA) at the animal pole, confocal imaging localizes paired spherical RNA clusters (black arrows), which are most likely associated with centrosomes; C — blastomeres AB and CD enter metaphase almost synchronously, maternal RNA is distributed as a diffuse cloud with distinct, bright clusters. These clusters are not dependent on the cell cycle phase but rather on the sample preparation (see main text). Staining: TO-PRO-1 (RNA, green), Hoechst 33342 (DNA, blue), Phalloidin-TRITC (F-actin; orange (A), yellow (B)).
White asterisk — reinfiltration of yolk protein granules. Abbreviations: pb — polar bodies.

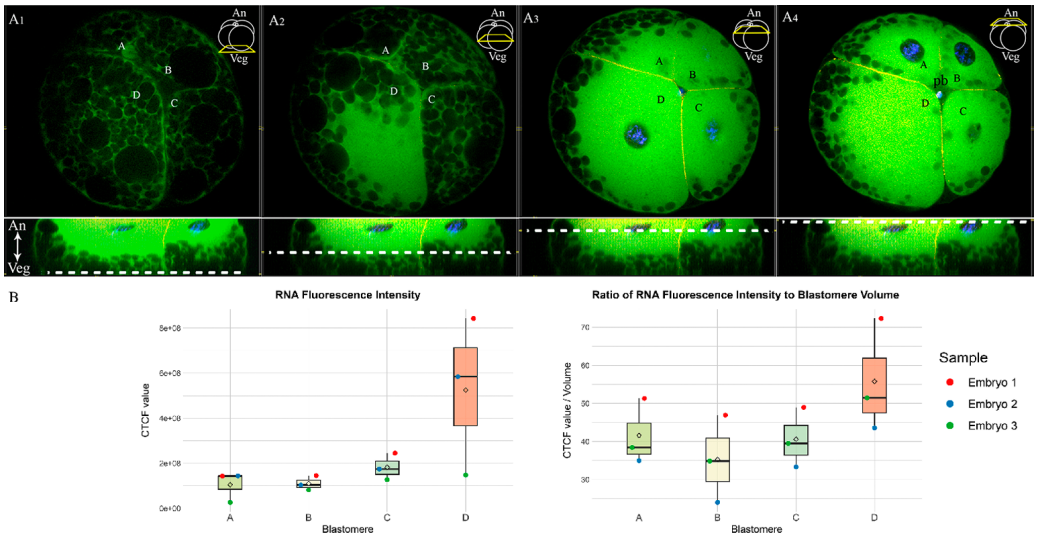

Fig. 5. Embryo at the 4-cell stage of *Platynereis dumerilii*. A1–A4 — optical sections across the animal-vegetal axis, with the positions of the sections indicated by white dashed lines; B — RNA fluorescence intensity (corrected total cell fluorescence, CTCF) in each blastomere and its relationship to blastomere volume, the highest concentration of maternal RNA is localized within the D blastomere. Staining: TO-PRO-1 (RNA, green), Hoechst 33342 (DNA, blue), Phalloidin-TRITC (F-actin, yellow).
Abbreviations: pb — polar bodies.

CLEAVAGE. 2-CELL STAGE (2–2.5 hpf). The first cleavage furrow follows the animal-vegetal axis, dividing the zygote into two unequal blastomeres — AB and CD. The larger blastomere, CD, contains 73% of the total ooplasm and retains 80% of the total amount of yolk-free cytoplasm (Dorresteijn, 1990). Maternal RNA is concentrated in the yolk-free cytoplasm at the animal pole, with the majority localized in the CD blastomere (Fig. 4A–C). Therefore, the qualitative disparity between the blastomeres in terms of maternal determinants is not proportional to their size. Dorresteijn describes the process of reinfiltration, referring to the re-entry of yolk protein granules into the clear cytoplasm of the CD blastomere, particularly in the region where the C blastomere will later form (Dorresteijn, 1990). We also observe this phenomenon, which, in our case, is facilitated by the strong contrast between the fluorescent RNA and the unstained yolk protein granules (Fig. 4B, white asterisk). The observed distribution of RNA is highly dependent on sample preparation. Specifically, in specimens stored in methanol and scanned immediately after staining, RNA forms a diffuse cloud interspersed with numerous distinct, bright clusters ranging from 2 to 10 μm in diameter (Fig. 4C). In contrast, only the shadows of these bright spots are visible in samples stained with phalloidin (i.e., not treated with alcohol) and mounted in Mowiol medium (Fig. 4A, hollow arrows). Interestingly, in our samples, RNA often forms paired spherical loci with a diameter of 12–13 μm (Fig. 4B). Their topology suggests an association with centrosomes. While the localization of centrosomes or microtubules is not addressed in this study, we highlight that such an association is both likely and expected. It is known that a significant pool of mRNA required for centrosome biogenesis is physically tethered to centrosomes and translated in situ (Safieddine *et al.*, 2021). Furthermore, specific RNAs, including maternal RNAs, may asymmetrically bind to centrioles, leading to asymmetric division and disparities in cell specialization (Lambert, Nagy, 2002).

We observed actin filaments in the nuclei of two-cell embryos (Fig. 4A). F-actin is synthesized in the nuclei of interphase cells during the G1 phase and is associated with postmitotic chromosome decondensation (Moore, Vartiainen, 2017).

4-CELL STAGE (3–3.5 hpf). The second cleavage furrow is oriented perpendicular to

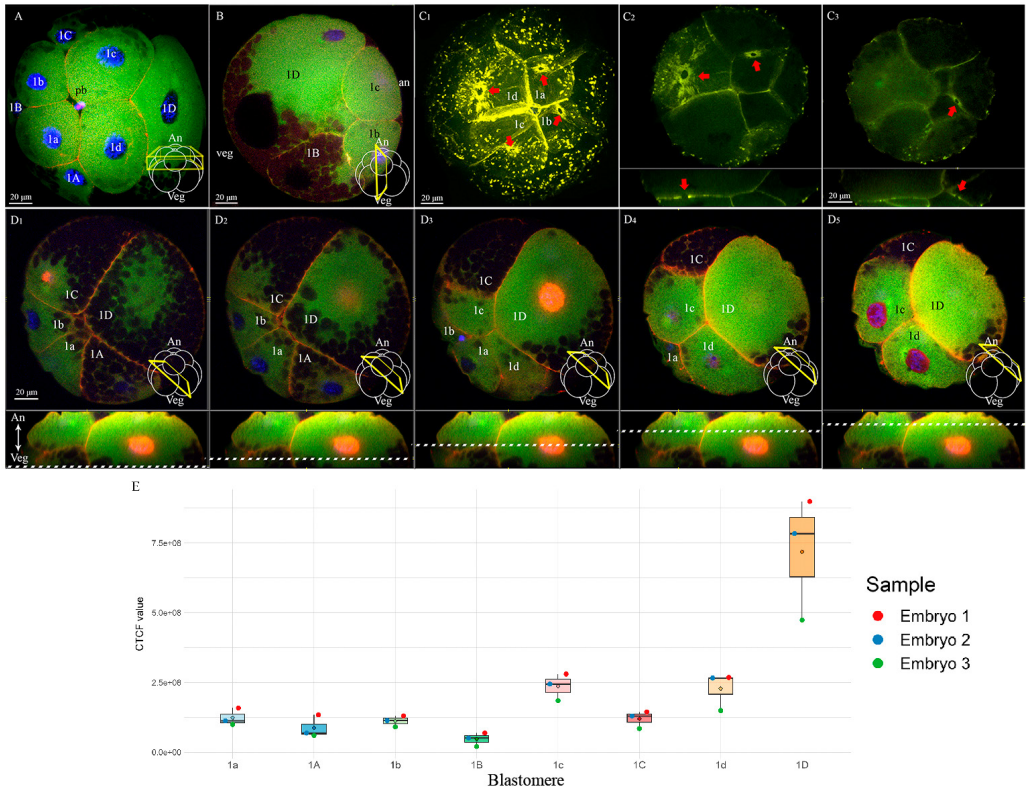

Fig. 6. Embryo at the 8-cell stage of *Platynereis dumerilii*. A — overview from the animal pole; B — lateral view, maternal RNA is not detected at the vegetal pole; C1–C3 — cytokinetic rings between blastomeres, nuclei are unstained, overview (C1) and individual optical sections (C2, C3), red arrows indicate cytokinetic rings; D1–D5 — optical sections along the animal-vegetal axis, positions of sections are indicated by white dashed lines, in all macromeres RNA surrounds the nuclei; E — RNA fluorescence intensity (corrected total cell fluorescence, CTCF) in each blastomere, the highest concentration of maternal RNA is segregated in the 1D blastomere. Staining: TO-PRO-1 (RNA, green), Hoechst 33342 (DNA, blue), Phalloidin-TRITC (F-actin; yellow in C1–C3, transitioning from orange to magenta depending on signal intensity in A, B, D1–D5). Abbreviation: pb — polar bodies.

the first, dividing the embryo into four founder blastomeres A, B, C, and D, which establish the primary cell lineages. The significant size difference between the C and D blastomeres influences the distribution of yolk protein granules and clear cytoplasm in distinct ways. Morphometric analyses (Dorresteijn, 1990) indicate that the yolk content of the C and D blastomeres differs by approximately twofold (15.44 and 29.86% of the total oocyte volume, respectively), whereas the clear cytoplasm content shows a threefold difference (6.52 and 21.04%, respectively). Maternal RNA, localized within the clear cytoplasm of the blastomeres, is predominantly enriched in the D blastomere (Fig. 5). RNA is distributed approximately equally between the A and B blastomeres (Fig. 5B). Confocal imaging further demonstrates that maternal RNA remains concentrated at the animal pole of the embryo. At the vegetal pole, yolk protein granules nearly displace the RNA-containing cytoplasm entirely.

8-CELL STAGE (4–4.5 hpf). During the third cleavage, each of the four blastomeres produces a descendant in the animal direction. The mitotic spindles are oriented clockwise (dexiotropic). This is the first "spiral" cleavage, and each formed micromere (1a–1d) is displaced relative to the macromeres (1A–1D) by approximately half of its own diameter (Fig. 6A). At this stage, yolk protein granules become more compact, and the

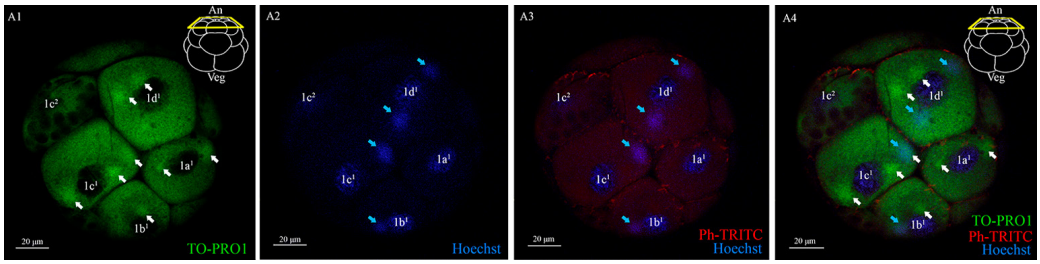

Fig. 7. Micromeres of the first quartet at the 16-cell stage of *Platynereis dumerilii*. A1 — a portion of the RNA forms aggregates surrounding the nuclei (white arrows); A2, A3, A4 — Hoechst-positive clusters (blue arrows; possibly mitochondrial clusters) occasionally overlap with RNA aggregates. Staining: TO-PRO-1 (RNA, green), Hoechst 33342 (DNA, blue), Phalloidin-TRITC (F-actin, red).

lipid droplets fuse, resulting in each macromere containing a single large lipid droplet cavity in the observed specimens. This process further displaces the clear cytoplasm, which harbors maternal RNA, toward the animal hemisphere (Fig. 6B). Macromeres 1A, 1B, and 1C transfer most of their RNA to corresponding micromeres. In contrast, macromere 1D contains such a substantial amount of RNA that, even after contributing to micromere 1d, 1D contains significantly more clear cytoplasm with RNA than any of the other macromeres (Fig. 6B; 6D1–D5).

According to morphometric data (Dorresteijn, 1990), macromeres differ in their contribution of clear cytoplasm to their descendants. This contribution is approximately equal for 1A and 1B (2.87 and 2.95%, respectively). However, the larger macromere 1C contributes a greater volume of cytoplasm to micromere 1c compared to macromere 1D's contribution to micromere 1d (5.44 and 4.54% of the total volume, respectively). This difference cannot be confirmed based on RNA fluorescence levels, as the distribution of RNA may follow different principles than that of the clear cytoplasm. Nevertheless, micromeres 1c and 1d generally exhibit slightly brighter TO-PRO1 staining compared to 1a and 1b. The maternal RNA retained in the macromeres is localized around the nuclei (Fig. 6D1–D5). Nuclear F-actin was detected in the nuclei of both macromeres and micromeres (Fig. 6D1–D5). Due to the brevity of the G1 phase in rapidly dividing cells, various stages of F-actin assembly were observed within the same embryo.

Blastomeres are known to enter the third mitosis asynchronously, with timing correlated to the amount of clear cytoplasm and, presumably, the cell-cycle-regulating factors it contains (Nakama *et al.*, 2017). As shown in Fig. 6F–J, blastomeres 1D and 1C, as well as their descendants (1d, 1c), have already reached the G-phase, in contrast to those in the A and B quadrants. A small subset of embryos in our study were fixed during the brief cytokinesis phase, when the cytokinetic ring at the boundaries between sibling blastomeres was still visible (Fig. 6F–J). This observation is particularly noteworthy, as the assembly and synchronization of the cytokinetic ring during cleavage in spiralians remain understudied.

16-CELL STAGE (5–5.5 hpf). The transition to this stage is characterized by a laeotropic (counterclockwise) division of the micromeres in the first quartet (1q) and a dexiotropic (clockwise) division of the macromeres. We examined the distribution of maternal RNA in two distinct planes of the 16-cell embryo (Fig. 7–9). In the animal pole daughter cells of the first quartet, $1a^1$, $1b^1$, $1c^1$, and $1d^1$ (collectively known as $1q^1$), a portion of the maternal RNA forms aggregates around the nuclei (Fig. 7A4). It is likely that this RNA is distributed on both sides of the future micromere cleavage plane and is associated with centrosomes. Furthermore, we observed loose Hoechst-positive clouds in these cells, indicating the formation of mitochondrial clusters that may be inherited in a determined manner (Fig. 7A2–A3; detailed image of clusters in Fig. S7). Interestingly, the vegetal pole daughter cells of the first quartet, $1a^2$, $1b^2$, $1c^2$, and $1d^2$ (collectively known as $1q^2$), contain less RNA and more yolk protein granules compared to $1q^1$ micromeres (Fig. 8A6–C).

During the fourth mitosis, the macromeres divide to form the second quartet of micromeres – 2a, 2b, 2c, and 2d. Macromere 1D produces

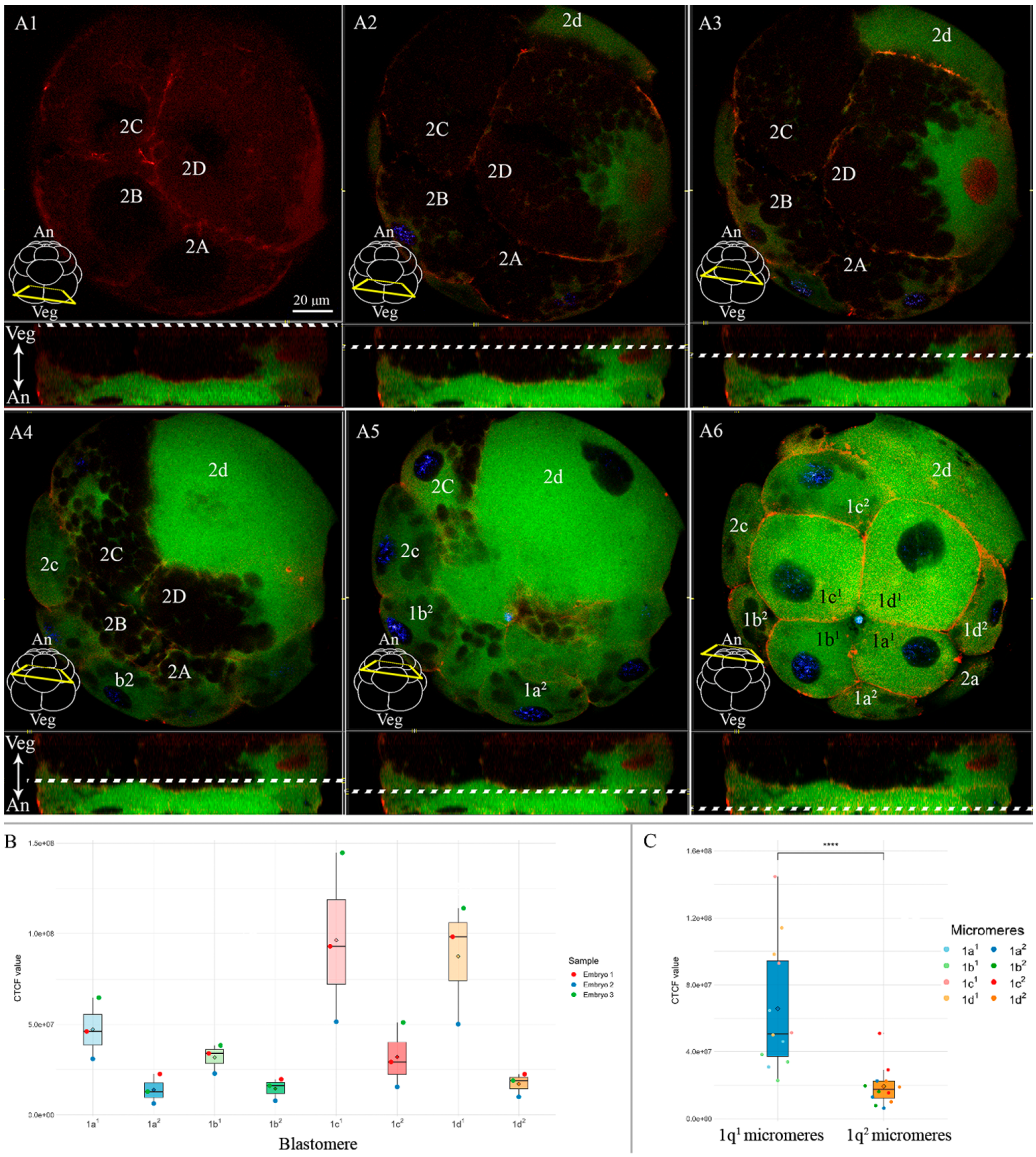

Fig. 8. Embryo at the 16-cell stage of *Platynereis dumerilii*. A — serial optical sections perpendicular to the animal-vegetal axis; A1 — according to our RNA staining, the vegetal poles of macromeres contain little or no RNA; A2–A5 — macromeres 2A–2D retain a small amount of RNA surrounding the nuclei, notably, the nucleus of 2D contains nuclear F-actin and is in the G1 phase; A4–A6 — the 2d micromere inherits nearly all of the RNA from 1D, becoming the largest cell in the embryo after 2D; A6 — micromeres $1a^1$–$1d^1$ are more enriched in maternal RNA than micromeres $1a^2$–$1d^2$; B — RNA fluorescence intensity (corrected total cell fluorescence, CTCF) in each daughter cell of the first quartet; C — RNA fluorescence intensity is higher in $1a^1$–$1d^1$ micromeres than $1a^2$–$1d^2$ (p-value = 3.328e-05). The positions of the sections are indicated by a white dashed line. Staining: TO-PRO-1 (RNA, green), Hoechst 33342 (DNA, blue), Phalloidin-TRITC (F-actin; red).

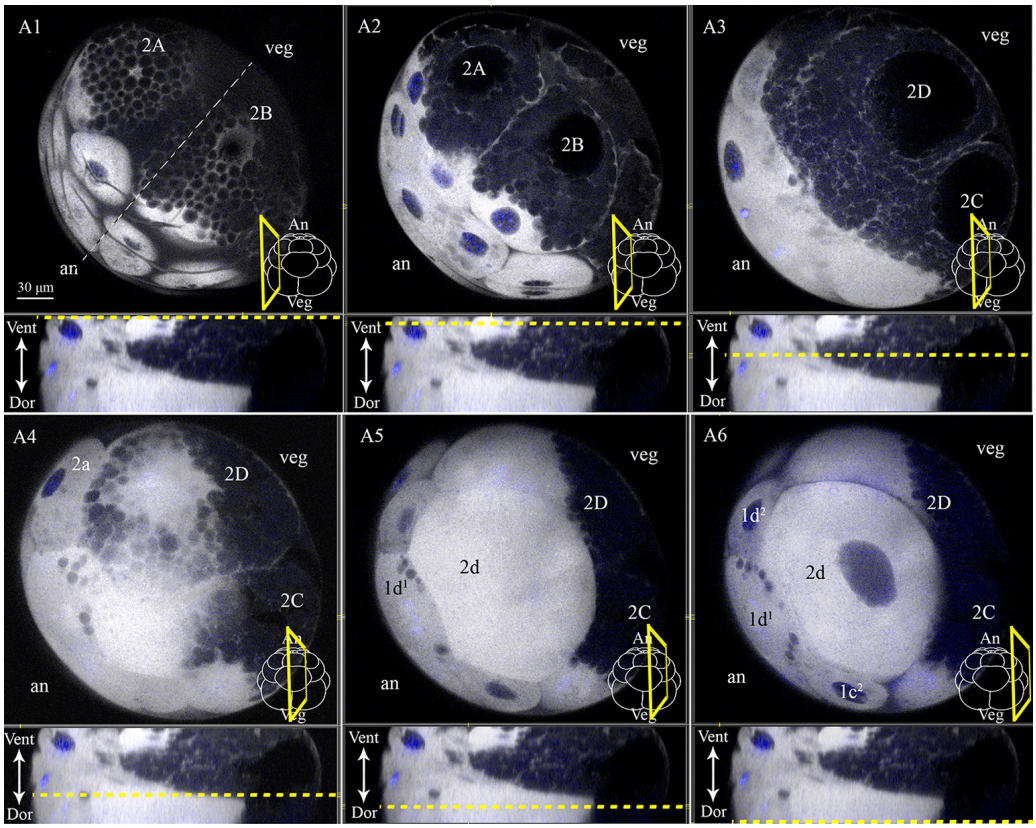

Fig. 9. Serial optical sections of *Platynereis dumerilii* 16-cell embryo, parallel to the animal-vegetal axis. A1, A2 — macromeres 2A and 2B contain small amounts of RNA in the perinuclear animal cytoplasm, devoid of yolk protein granules and large lipid cavities (dark spherical bodies in each macromere, proportional to their size); A3, A4 — macromeres 2C and 2D, their nuclei are absent in this series of sections; A5, A6 — the 2d micromere, with a large nucleus, contains the highest amount of maternal RNA among all blastomeres. The positions of the sections are indicated by a yellow dashed line. Staining: TO-PRO-1 (RNA, white), Hoechst 33342 (DNA, blue).

the largest micromere of this quartet, 2d, also referred to as the "first somatoblast". The 2d micromere will later give rise to all ectodermal derivatives of the larva and adult worm, with the exceptions of the head, which originates from the first quartet of micromeres, and the narrow band of posttrochal epidermis, which is formed by $2a^1$–$2c^1$ micromeres (Ackermann *et al.*, 2005). The 2d micromere is larger than all the macromeres, with the exception of the 2D, and harbors the majority of the maternal RNA inherited from 1D (Figs 8; 9). It contains no yolk protein granules or lipid droplet cavities. This micromere contains a large elliptical nucleus (~40 µm along the long axis), with dimensions approaching those of the micromeres $1a^2$–$1d^2$ (Fig. 9A6). Dorresteijn's study demonstrated that the nucleus contains numerous spherical inclusions resembling nucleoli (Dorresteijn, 1990). A small amount of maternal RNA remains in all four macromeres, localized around the nuclei (Figs 8A2–A5; 9A1–A2). Notably, except for the 2d micromere, the micromeres $1a^1$–$1d^1$ appear to be the most enriched in RNA at this stage.

Discussion

The study of the early development in nereid annelids has a long history, beginning in the late 19th century with the classic work of E.B. Wilson (Wilson, 1892). The morphology and cytological features of *P. dumerilii* oocytes and early embryos

Table 2. Comparison of mean total RNA content per oocyte across various animal species.

Group	Organism	Mean RNA per egg (ng)	Mean diameter (μm)	Reference
Vertebrates	Average mammalian cell	0.015	10–20	(Morgado *et al.*, 1990; Russo, 2014)
	Homo sapiens	0.33	110–120	(Kocabas *et al.*, 2006; Nazari *et al.*, 2011)
	Mus musculus	0.35	89.9	(Piko, Clegg, 1982; Eppig, Schroeder, 1989)
	Sus domesticus	0.65	110–120	(Olszanska, Borgul, 1993; Hunter, 2000)
	Ovis aries	0.76	110–150	(Olszanska, Borgul, 1993; Shirazi, Sadeghi, 2007)
	Bos taurus	0.93–2	110–120	(Olszanska, Borgul, 1993; Lequarre *et al.*, 2004; Rotar, Souza, 2019)
	Oryctolagus cuniculus	6–15	113.93	(Piko, Clegg, 1982; Olszanska, Borgul, 1993; Hadjadj *et al.*, 2024)
	Gallus domesticus	2100	40 000	(Olszanska, Borgul, 1993; Nishio *et al.*, 2018)
	Xenopus laevis	4800	1300	(Taylor *et al.*, 1985; Mowry, 2020)
	Xenopus tropicalis	1000	700	(Marchant, Parker, 2001; Talhouarne, Gall, 2014)
	Triturus cristatus	8500	2000	(Davidson, 1986; Fudula *et al.*, 2008)
Echinoderms	*Tripneustes gratilla*	1.7	50–60	(Duncan, Humphreys, 1981; AbouElmaaty *et al.*, 2023)
	Arbacia punctulata	2.3	29.2–69.8	(Kovesdi, Smith, 1982; Hernandez *et al.*, 2020)
	Strongylocentrotus purpuratus	2.8	60–70	(Chatlynne, 1971; Goustin, Wilt, 1981)
	Lytechinus pictus	3.9	110	(Brandhorst, 1980; Nesbit *et al.*, 2019)
	Dendraster excentricus	4.8	88.6–187.6	(Mizuno *et al.*, 1973; Olivares-Baņuelos *et al.*, 2012)
	Pisaster ochraceus	15	200	(Mauzey, 1966; Kovesdi, Smith, 1982)
Annelids	*Platynereis dumerilii*	10.17	150–180	Current study
	Urechis caupo	14	110–115	(Gould-Somero, Holland, 1975; Davidson, 1986)
Insects	*Drosophila melanogaster*	190	290–320	(Imai, 1934; Anderson, Lengyel, 1979)
	Musca domestica	1200	1200	(Hough-Evans *et al.*, 1980; Sanchez-Arroyo, Capinera, 2003)

have been described in detail in previous studies (Dorresteijn, 1990; Fischer *et al.*, 2010; Hsieh, 2020; Özpolat *et al.*, 2021), and are therefore not the focus of our work. We note, however, that even in our local analysis, conducted with minimal tools (phalloidin and nucleic acid dyes), the complex F-actin architecture is clearly visible, including high dynamic assembly and disassembly of nuclear actin and cytokinetic rings. In this study, we expand upon this foundation by quantifying and visualizing, for the first time, the total maternal RNA content and its localization in *P. dumerilii* oocytes and early embryos.

We found that a single worm oocyte contains approximately 10 ng of RNA. Could this parameter reveal meaningful patterns in evolution and development? We suggest it is likely too variable to serve as a reliable comparative measure. Among deuterostomes, which have been most extensively studied in this context, there is substantial variation in RNA content per oocyte. Mature murine oocytes contain approximately 0.35 ng of total RNA, while human oocytes contain around 0.33 ng. Rabbit oocytes have an RNA content ranging from 6 to 15 ng, and chicken oocytes contain about 2.1 μg of RNA. Notably, *Xenopus laevis* and *X. tropicalis* differ fourfold in RNA content (~4 μg and 1 μg, respectively). Studied echinoderms exhibit an average RNA content of between 1.7 and 15 ng per oocyte, whereas in insects (Diptera) the amount ranges from 190 ng (*Drosophila melanogaster*) to 1.2 μg (*Musca domestica*) (see Table 2). Importantly, in spiralians, maternal RNA composition is associated with developmental polymorphism, known as poecilogony. For example, the annelid *Streblospio benedicti* (Spionidae) produces differently sized oocytes with varying RNA compositions, giving rise to morphologically distinct larvae occupying separate ecological niches. Specifically, smaller eggs develop into obligate planktotrophic larvae, while larger eggs yield lecithotrophic or facultatively planktotrophic larvae (Pernet, McArthur, 2006; Harry, Zakas, 2023). Thus, maternal RNA investment varies considerably both between and within species (poecilogony), reflecting significant evolutionary plasticity.

The total amount of maternal RNA likely correlates with the number of cell cycles preceding MZT. Indeed, in mammals, which have relatively low levels of maternal RNA, zygotic genome activation occurs at the 2–4 blastomere stage (24–48 hpf). In contrast, echinoderms, fish, amphibians and insects, which possess abundant maternal RNA, initiate zygotic transcription at the multicellular stage, specifically during the mid-blastula transition (MBT) (Winata, Korzh, 2018; Vastenhouw *et al.*, 2019). In this context, *P. dumerilii* resembles echinoderms and echiurans (Table 2), which exhibit late MZT waves (Franks, Davis, 1983; Matsushita *et al.*, 2017; Kipryushina, Yakovlev, 2020). Consistent with this, in *P. dumerilii*, zygotic genome activation begins during late cleavage (~30 cells) and is completed by the blastula stage (~140 cells) (Chou *et al.*, 2016).

To initiate zygotic genome activation, animals may employ one of two strategies: depleting repressors and/or accumulating activators. In fish and amphibians, zygotic genome activation is triggered upon reaching a critical nuclear-to-cytoplasmic (N/C) ratio, which increases during cleavage. Ultimately, depletion of maternal suppressors (e.g., histones) initiates transcription (Amodeo *et al.*, 2015). In *P. dumerilii*, however, the large 2d micromere displays early markers of zygotic genome activation (asynchronous cleavage, bilateral division pattern, nucleolus-like structures) despite having a significantly lower N/C ratio than other micromeres (Dorresteijn, 1990). This suggests that in *P. dumerilii*, zygotic genome activation in 2d micromere may be regulated independently of the global N/C threshold.

In *P. dumerilii*, zygotic genome activation may be triggered by chromatin accessibility to transcriptional activators rather than by repressor depletion. This mechanism, best characterized in mammals, involves pluripotency factors, such as DUX4, OCT4, NF-Y, SoxB1, and Nanog (Schulz, Harrison, 2019). In addition, clearance of maternal RNA is essential for genome activation. The Smaug/Samd4 factor is crucial for activating "anti-maternal" microRNAs that directly degrade subsets of maternal mRNAs (Benoit *et al.*, 2009; Luo *et al.*, 2016). Transcriptomic data from *P. dumerilii* (Chou *et al.*, 2016, Supplementary) reveal the presence of maternal *NF-Y* and *Smaug* ortholog transcripts by the 6–8 hpf developmental stage. These findings make it reasonable to hypothesize that *P. dumerilii* employs evolutionarily conserved MZT pathways, although functional validation is required to confirm this.

We observe that in *P. dumerilii* oocytes, most RNA is concentrated in the perinuclear ooplasm,

an area free of yolk protein granules and lipid droplets, with a smaller fraction dispersed toward the periphery. During cleavage, maternal RNA shifts to the animal pole and surrounds the blastomere nuclei. This pattern contrasts sharply with that of the annelid *Chaetopterus* (Jeffery, Wilson, 1983), where maternal RNA is distributed peripherally in the ectoplasm and remains associated with the cortex in both oocytes and blastomeres. In *Chaetopterus*, RNA at the animal pole is distributed equally between AB and CD blastomeres, while vegetal RNA predominantly localizes to the CD lineage (Jeffery, Wilson, 1983). The phylogenetically distant *Platynereis* and *Chaetopterus* may use distinct mechanisms for maternal RNA packaging and segregation, reflecting independent evolutionary paths. Their differing reproductive strategies are also noteworthy. While *Chaetopterus* larvae begin feeding as metatrochophores by 36 hpf (Irvine *et al.*, 1999), *P. dumerilii* exhibits lecithotrophic development, with larvae starting to feed only after 5–7 days as mature nectochaetes. Unlike *Chaetopterus*, *P. dumerilii* oocytes accumulate additional components, such as large lipid droplets and small yolk protein granules. The spatial organization of oocytes may follow principles similar to the mathematical concept of the Packing Problems rather than clade-specific developmental rules.

In our study, we did not perform a comparative assessment of RNA staining intensity across stages, but we did not observe significant changes between the oocyte, zygote, and cleavage stages. This may suggest that the most abundant maternal RNA species degrade after the 16-cell stage (5–5.5 hpf). Indeed, transcriptomic data indicate that maternal ribosomal RNAs — among the most abundant RNAs in the oocyte — are eliminated between 8 and 10 hpf (Chou *et al*., 2016)

In *P. dumerilii,* maternal RNA forms a distinct "star-shaped" pattern in perinuclear cytoplasm of oocyte. This distribution matches the localization of specific mRNAs (*Pdum-twist*, *Pdum-vasa*, ACDs, Hox genes) visualized by in situ hybridization (Pfeifer *et al.*, 2014; Nakama *et al.*, 2017; Maslakov *et al.*, 2021; Kuehn *et al.*, 2022). However, *Pdum-acox3* (Acyl-Coenzyme A oxidase 3) transcripts localize preferentially to one oocyte pole (Maslakov *et al.*, 2021, Supplementary), representing the only known example of anisotropic RNA distribution in *P. dumerilii*. The star-shaped pattern is RNase-sensitive, suggesting that fragmented RNA may diffuse more readily after losing stabilizing interactions with proteins. The absence of TO-PRO-1 fluorescence in the egg jelly layer of RNase-treated oocytes (Fig. 2C–C1) further supports the idea of enhanced diffusion under these conditions.

During spiral cleavage, maternal RNA is not randomly distributed among blastomeres. By the 16-cell stage, it is most highly concentrated in the first quartet micromeres $1a^1$–$1d^1$ ($1q^1$) and in the first somatoblast 2d. The descendants of the $1q^1$ cells will form the cerebral ganglion, sensory organs, head epithelium, and accessory trochoblasts, while the progeny of 2d blastomere contribute to the trunk nervous system and trunk integument (Ackermann *et al.*, 2005). These cells differ from other blastomeres in two ways. First, they generate a very large number of progeny before the larva starts feeding. Second, their progeny gives rise to nearly all ectodermal tissues in the adult animal (in case of 1q1 and 2d) or become part of the growth zone that generates the postlarval body (in case of 2d) (Ackermann *et al.*, 2005). Notably, the blastomeres $1a^2$–$1d^2$ ($1q^2$) contain significantly less maternal RNA than their sister $1q^1$ cells. They divide only twice, resulting in cell lineages $1q^{222}$, $1q^{221}$, $1q^{212}$, $1q^{211}$, and then terminally differentiate into the provisional organ, prototroch. We hypothesize that these differences in cell fate among early *P. dumerilii* blastomeres are linked to the asymmetric segregation of maternal RNA.

In a detailed study by Dorresteijn (1990), it was shown that the ratio of yolk to free cytoplasm is both individual and stereotypical for blastomeres in early *P. dumerili* embryos, and that it correlates with cell cycle length. Specifically, the greater the amount of free cytoplasm, the earlier the cell enters mitosis. Additionally, the volume of free cytoplasm correlates with nuclear size. We suggest that this free cytoplasm largely corresponds to the RNA-containing cytoplasm observed in our study.

Thus, our study reveals that *P. dumerilii* oocytes contain abundant maternal RNA, though interspecies variability limits its evolutionary interpretability. Unlike *Chaetopterus*, *P. dumerilii* RNA localizes perinuclearly in a "star-shaped" pattern, consistent with prior reports of *Twist*, *Vasa*, and *Hox* transcripts. The distribution of total maternal RNA is dynamic, non-random, and closely linked to patterns of spiral cleavage. These findings provide a valuable foundation for comparative and experimental studies on maternal contributions to the regulation of early

development in spiralians, as well as for future research on the MZT.

Compliance with ethical standards

CONFLICTS OF INTEREST: The authors declare that they have no conflicts of interest.

Supplementary data. The following materials are available online.

File S1. CTAB-based total RNA isolation protocol.

File S2. Quantification of RNA Fluorescence: Computed Values.

Fig. S1. Agarose gel electrophoresis with extracted oocyte RNA.

Fig. S2. Image of oocytes labeled using the DL-gram cloud service.

Fig. S3. Complete series of histological sections of P. dumerilii zygotes (0.5 hpf) stained with Carazzi's hematoxylin and eosin.

Fig. S4. Control for autofluorescence in the TO-PRO-1 channel (Ex/Em: 515/531 nm).

Fig. S5. Nechtochate larva, stained with primary anti-acetylated tubulin antibodies and secondary antibodies (anti-mouse CF633).

Fig. S6. Figure 3 with the tubulin channel. Zygotes (0.5 hpf).

Fig. S7. Embryos at the stage of 16 cells, stained with Hoechst and Phalloidin-TRITC. Putative mitochondrial clusters are shown.

Acknowledgements. The research was supported by the Russian Science Foundation, grant number 23-24-00426. The authors are grateful to the "Chromas" resource center at SPbU for providing access to the Leica DMRXA workstation, the Leica TCS SP5 Confocal Laser Scanning Microscope, Bitplane Imaris 7.7.0 and Adobe Photoshop CS 5.1 software. The authors also thank the Research Resource Center "Centre for Molecular and Cell Technologies of SPbSU" for access to the Leica SM-2010R sliding microtome and the Leica DMI6000 microscope. We thank Aazad Mohamed Mohamed Nazeem, PhD student at the Okinawa Institute of Science and Technology, for his invaluable assistance in editing the English syntax and grammar in the Introduction, Discussion, and Methods sections.

References

AbouElmaaty E., Yassien M., Hanafy M., Ghobashy A., Ahmed M., Baeta M. 2023. Reproductive aspects of the sea urchin *Tripneustes gratilla* from the Red Sea, Egypt // Egypt. J. Aquat. Biol. Fish. Vol.27. P.475–494.

Ackermann C., Dorresteijn A., Fischer A. 2005. Clonal domains in postlarval *Platynereis dumerilii* (Annelida: Polychaeta) // J. Morphol. Vol.266. P.258–280. DOI: 10.1002/jmor.10375

Amodeo A.A., Jukam D., Straight A.F., Skotheim J.M. 2015. Histone titration against the genome sets the DNA-to-cytoplasm threshold for the *Xenopus* midblastula transition // Proc. Natl. Acad. Sci. USA. Vol.112. P.E1086-E1095

Anderson K.V., Lengyel J.A. 1979. Rates of synthesis of major classes of RNA in *Drosophila* embryos // Dev. Biol. Vol.70. P.217–231. DOI: 10.1016/0012-1606(79)90018-6

Benoit B., He C.H., Zhang F., Votruba S.M., Tadros W., Westwood J.T., Smibert C.A., Lipshitz H.D., Theurkauf W.E. 2009. An essential role for the RNA-binding protein Smaug during the *Drosophila* maternal-to-zygotic transition // Development. Vol.136. P.923–932. DOI: 10.1242/dev.031815

Bolte S., Cordelières F.P. 2006. A guided tour into subcellular colocalization analysis in light microscopy // J. Microsc. Vol.224. P.213–232. DOI: 10.1111/j.1365-2818.2006.01706.x

Brandhorst B.P. 1980. Simultaneous synthesis, translation, and storage of mRNA including histone mRNA in sea urchin eggs // Dev. Biol. Vol.79. P.139–148. DOI: 10.1016/0012-1606(80)90079-2

Briggs R., Green E.U., King T.J. 1951. An investigation of the capacity for cleavage and differentiation in *Rana pipiens* eggs lacking "functional" chromosomes // J. Exp. Zool. Vol.116. P.455–499. DOI: 10.1002/jez.1401160307

Chatlynne L.G. 1971. An ultrastructure study of oogenesis in the sea urchin, *Strongylocentrotus purpuratus*. Thesis of Candidate (Ph.D.) of Biological Sci. Degree. Corvallis: Oregon State University. 144 p.

Chou H.-C., Pruitt M.M., Bastin B.R., Schneider S.Q. 2016. A transcriptional blueprint for a spiral-cleaving embryo // BMC Genomics. Vol.17. P.1–25. DOI: 10.1186/s12864-016-2860-6

Davidson E.H. 1986. Gene Activity in Early Development (Third Edition). San Diego: Academic Press. 670 p.

Davidson E.H., Britten R.J. 1979. Regulation of gene expression: possible role of repetitive sequences // Science. Vol.204. P.1052–1059. DOI: 10.1126/science.451548.

Dorresteijn A.W. 1990. Quantitative analysis of cellular differentiation during early embryogenesis of *Platynereis dumerilii* // Roux's Archives of Development Biology. Vol.199. P.14–30. DOI: 10.1007/BF01681530

Duncan R., Humphreys T. 1981. Most sea urchin maternal mRNA sequences in every abundance class appear in both polyadenylated and nonpolyadenylated molecules // Dev. Biol. Vol.88. P.201–210. DOI: 10.1016/0012-1606(81)90164-0

Eppig J.J., Schroeder A.C. 1989. Capacity of mouse oocytes from preantral follicles to undergo embryogenesis and development to live young after growth, maturation, and fertilization in vitro // Biol. Reprod. Vol.41. P.268–276. DOI: 10.1095/biolreprod41.2.268

Fischer A.H., Dorresteijn A. 2004. The polychaete *Platynereis dumerilii* (Annelida): a laboratory animal with spiralian cleavage, lifelong segment proliferation and a mixed benthic/pelagic life cycle // BioEssays. Vol.26. P.314–325. DOI: 10.1002/bies.10409

Fischer A.H., Henrich T., Arendt D. 2010. The normal development of *Platynereis dumerilii* (Nereididae, Annelida) // Front. Zool. Vol.7. Art.31. DOI: 10.1186/1742-9994-7-31

Franks R.R., Davis F.C. 1983. Regulation of histone synthesis during early *Urechis caupo* (Echiura) development // Dev. Biol. Vol.98. P.101–109. DOI: 10.1016/0012-1606(83)90338-x

Fudula M., Ivanović A., Dgukic G., Kalezić M.L. 2008. Egg Size Variation in Crested Newts from the Western Balkans (Caudata: Salamandridae: *Triturus cristatus* Superspecies) // Zool. Stud. Vol.47. P.585–590.

Ghawana S., Paul A., Kumar H., Kumar A., Singh H., Bhardwaj P.K., Rani A., Singh R.S., Raizada J., Singh K., Kumar S. 2011. An RNA isolation system for plant tissues rich in secondary metabolites // BMC Res. Notes. Vol.4. Art.85. DOI: 10.1186/1756-0500-4-85

Gould-Somero M., Holland L. 1975. Oocyte differentiation in *Urechis caupo* (Echiura): a fine structural study // J. Morphol. Vol.147. P.475–505. DOI: 10.1002/jmor.1051470407

Goustin A.S., Wilt F.H. 1981. Protein synthesis, polyribosomes, and peptide elongation in early development of *Strongylocentrotus purpuratus* // Dev. Biol. Vol.82. P.32–40. DOI: 10.1016/0012-1606(81)90426-7

Hadjadj I., Zuzana F., Luz G.M.d.l., Barbora L., Martin M., Peter M., Ivan A., Sirotkin A.V., Argente M.J. 2024. Effects of selection for litter size variability on ovarian folliculogenesis, ovarian cell proliferation, apoptosis, and production of regulatory peptides in rabbits // Ital. J. Anim. Sci. Vol.23. P.1290–1304. DOI: 10.1080/1828051X.2024.2396482

Hardege J.D., Müller C.T., Beckmann M., Bartels-Hardege H.D., Bentley M.G. 1998. Timing of reproduction in marine polychaetes: The role of sex pheromones // Écoscience. Vol.5. P.395–404. DOI: 10.1080/11956860.1998.11682477

Harry N.D., Zakas C. 2023. Maternal patterns of inheritance alter transcript expression in eggs // BMC Genomics. Vol.24. Art.191. DOI: 10.1186/s12864-023-09291-8

Hernandez E., Vázquez O.A., André T., Rahman M.S. 2020. Reproductive cycle and gonadal development of the Atlantic sea urchin *Arbacia punctulata* in the Gulf of Mexico: changes in nutritive phagocytes in relation to gametogenesis // Mar. Biol. Res. Vol.16. P.177–194. DOI: 10.1080/17451000.2020.1731758

Hough-Evans B.R., Jacobs-Lorena M., Cummings M.R., Britten R.J., Davidson E.H. 1980. Complexity of RNA in eggs of *Drosophila melanogaster* and *Musca domestica* // Genetics. Vol.95. P.81–94. DOI: 10.1093/genetics/95.1.81

Hsieh Y.W. 2020. Cellular, cytoskeletal, and biophysical mechanisms of spiral cleavage during *Platynereis dumerilii* Embryogenesis. Thesis of Candidate (Ph.D.) of Biological Sci. Degree. Dresden: Tech. Univ. 305 p.

Hunter M.G. 2000. Oocyte maturation and ovum quality in pigs // Biol. Reprod. Vol.5. P.122–130. DOI: 10.1530/ror.0.0050122

Imai T. 1934. The influence of temperature on egg size and variation in *Drosophila melanogaster* // Wilhelm Roux Arch. Entwickl. Mech. Org. Vol.132. P.206–219. DOI: 10.1007/BF00579868

Irvine S.Q., Chaga O., Martindale M.Q. 1999. Larval ontogenetic stages of *Chaetopterus*: developmental heterochrony in the evolution of chaetopterid polychaetes // Biol. Bull. Vol.197. P.319–331. DOI: 10.2307/1542786

Jeffery W.R., Wilson L.J. 1983. Localization of messenger RNA in the cortex of *Chaetopterus* eggs and early embryos // Development. Vol.75. P.225–239.

Kipryushina Y.O., Yakovlev K.V. 2020. Maternal control of early patterning in sea urchin embryos // Differentiation. Vol.113. P.28–37. DOI: 10.1016/j.diff.2020.04.001

Kiss T., Karácsony Z., Gomba-Tóth A., Szabadi K.L., Spitzmüller Z., Hegyi-Kaló J., Cels T., Otto M., Golen R., Hegyi Á.I., Geml J., Váczy K.Z. 2024. A modified CTAB method for the extraction of high-quality RNA from mono-and dicotyledonous plants rich in secondary metabolites // Plant Methods. Vol.20. Art.62. DOI: 10.1186/s13007-024-01198-z

Kluge B., Lehmann-Greif M., Fischer A. 1995. Long-lasting exocytosis and massive structural reorganisation in the egg periphery during cortical reaction in *Platynereis dumerilii* (Annelida, Polychaeta) // Zygote. Vol.3. P.141–156. DOI: 10.1017/s0967199400002513

Kocabas A.M., Crosby J., Ross P.J., Otu H.H., Beyhan Z., Can H., Tam W.-L., Rosa G.J.M., Halgren R.G., Lim B., Fernandez E., Cibelli J.B. 2006. The transcriptome of human oocytes // Proc. Natl. Acad. Sci. USA. Vol.103. P.14027–14032. DOI: 10.1073/pnas.0603227103

Kovesdi I., Smith M.J. 1982. Sequence complexity in the maternal RNA of the starfish *Pisaster ochraceus* (Brandt) // Dev. Biol. Vol.89. P.56–63. DOI: 10.1016/0012-1606(82)90293-7

Kuehn E., Clausen D.S., Null R.W., Metzger B.M., Willis A.D., Özpolat B.D. 2022. Segment number threshold determines juvenile onset of germline cluster expansion in *Platynereis dumerilii* // J. Exp. Zool. Vol.338. P.225–240. DOI: 10.1002/jez.b.23100

Lambert J.D., Nagy L.M. 2002. Asymmetric inheritance of centrosomally localized mRNAs during embryonic cleavages // Nature. Vol.420. P.682–686. DOI: 10.1038/nature01241

Lemon J. 2006. Plotrix: A package in the red light district of R // R-News. Vol.6. P.8–12.

Lequarre A.S., Traverso J.M., Marchandise J., Donnay I. 2004. Poly(A) RNA Is Reduced by Half During Bovine Oocyte Maturation but Increases when Meiotic Arrest Is Maintained with CDK Inhibitors1 // Biol. Reprod. Vol.71. P.425–431. DOI: 10.1095/biolreprod.103.026724

Liu M.M., Davey J.W., Jackson D.J., Blaxter M.L., Davison A. 2014. A conserved set of maternal genes? Insights from a molluscan transcriptome // Int. J. Dev. Biol. Vol.58. P.501–511. DOI: 10.1387/ijdb.140121ad

Luo H., Li X., Claycomb J.M., Lipshitz H.D. 2016. The Smaug RNA-Binding Protein Is Essential for microRNA Synthesis During the *Drosophila* Maternal-to-Zygotic Transition // G3: Genes Genomes Genet. Vol.6. P.3541–3551. DOI: 10.1534/g3.116.034199

Marchant J.S., Parker I. 2001. *Xenopus tropicalis* oocytes as an advantageous model system for the study of intracellular Ca(2+) signalling // Br. J. Pharmacol. Vol.132. P.1396–1410. DOI: 10.1038/sj.bjp.0703922

Maslakov G.P., Kulishkin N.S., Surkova A.A., Kulakova M.A. 2021. Maternal Transcripts of Hox Genes Are Found in Oocytes of *Platynereis dumerilii* (Annelida, Nereididae) // J. Dev. Biol. Vol.9. DOI: 10.3390/jdb9030037

Matsushita M., Ochiai H., Suzuki K.T., Hayashi S., Yamamoto T., Awazu A., Sakamoto N. 2017. Dynamic changes in the interchromosomal interaction of early histone gene loci during development of sea urchin // J. Cell Sci. Vol.130. P.4097–4107. DOI: 10.1242/jcs.206862

Matveev A.V., Nartova A.V., Sankova N.N., Okunev A.G. 2024. DLgram cloud service for deep-learning analysis of microscopy images // Microsc. Res. Tech. Vol.87. P.991–998. DOI: 10.1002/jemt.24480

Mauzey K.P. 1966. Feeding Behavior and Reproductive Cycles in *Pisaster ochraceus* // Biol. Bull. Vol.131. P.127–144. DOI: 10.2307/1539653

Metzger B., Özpolat B.D. 2024. The cost and payout of age on germline regeneration and sexual

maturation in *Platynereis dumerilii* // bioRxiv. DOI: 10.1101/2024.01.22.576726

Mizuno S., Whiteley H.R., Whiteley A.H. 1973. The Enrichment of Egg-type RNA in Cleavage Stage Embryos of the Sand Dollar *Dendraster excentricus* // Differentiation. Vol.1. P.339–348. DOI: 10.1111/j.1432-0436.1973.tb00130.x

Moore H.M., Vartiainen M.K. 2017. F-actin organizes the nucleus // Nat. Cell Biol. Vol.19. P.1386–1388. DOI: 10.1038/ncb3650.

Morgado E., Ocqueteau C., Cury M., Becker L., González U., Muxica L., Günther B. 1990. Three-dimensional morphometry of mammalian cells. II. Areas, volumes, and area-volume ratios // Arch. Biol. Med. Exp. Vol.23. P.21–27.

Mowry K.L. 2020. Using the *Xenopus* Oocyte Toolbox // Cold Spring Harb. Protoc. Vol.2020. Art.095844. DOI: 10.1101/pdb.top095844

Nakama A.B., Chou H.-C., Schneider S.Q. 2017. The asymmetric cell division machinery in the spiral-cleaving egg and embryo of the marine annelid *Platynereis dumerilii* // BMC Dev. Biol. Vol.17. Art.16. DOI: 10.1186/s12861-017-0158-9

Nazari S., Khalili M.A., Esmaielzadeh F., Mohsenzadeh M. 2011. Maturation capacity, morphology and morphometric assessment of human immature oocytes after vitrification and in-vitro maturation // Iran. J. Reprod. Med. Vol.9. P.209–216.

Nesbit K.T., Fleming T., Batzel G., Pouv A., Rosenblatt H.D., Pace D.A., Hamdoun A., Lyons D.C. 2019. Chapter 5 - The painted sea urchin, *Lytechinus pictus*, as a genetically-enabled developmental model // K.R. Foltz, A. Hamdoun (eds.). Methods in Cell Biology. Academic Press. Тщю150. P.105–123.

Nishio S., Okumura H., Matsuda T. 2018. Egg-Coat and Zona Pellucida Proteins of Chicken as a Typical Species of Aves // Curr. Top. Dev. Biol. Vol.130. P.307–329. DOI: 10.1016/bs.ctdb.2018.02.008

Olivares-Baṇuelos T., Figueroa-Flores S., Carpizo-Ituarte E. 2012. Gonad index and larval development of the sand dollar *Dendraster excentricus* (Echinodermata; Echinoidea) in Baja California, Mexico // Cienc. Mar. Vol.38. P.411–425.

Olszanska B., Borgul A. 1993. Maternal RNA content in oocytes of several mammalian and avian species // J. Exp. Zool. Vol.265. P.317–320. DOI: 10.1002/jez.1402650313

Özpolat B.D., Randel N., Williams E.A., Bezares-Calderón L.A., Andreatta G., Balavoine G., Bertucci P.Y., Ferrier D.E.K., Gambi M.C., Gazave E., Handberg-Thorsager M., Hardege J., Hird C., Hsieh Y.-W., Hui J., Mutemi K.N., Schneider S.Q., Simakov O., Vergara H.M., Vervoort M., Jékely G., Tessmar-Raible K., Raible F., Arendt D. 2021. The Nereid on the rise: *Platynereis* as a model system // EvoDevo. Vol.12. Art.10. DOI: 10.1186/s13227-021-00180-3

Pernet B., McArthur L. 2006. Feeding by larvae of two different developmental modes in *Streblospio benedicti* (Polychaeta: Spionidae) // Mar. Biol. Vol.149. P.803–811. DOI: 10.1007/s00227-006-0266-8

Pfeifer K., Schaub C., Domsch K., Dorresteijn A., Wolfstetter G. 2014. Maternal inheritance of twist and analysis of MAPK activation in embryos of the polychaete annelid *Platynereis dumerilii* // PLoS One. Vol.9. Art.e96702. DOI: 10.1371/journal.pone.0096702

Piko L., Clegg K.B. 1982. Quantitative changes in total RNA, total poly(A), and ribosomes in early mouse embryos // Dev. Biol. Vol.89. P.362–378. DOI: 10.1016/0012-1606(82)90325-6

Röhl I., Schneider B., Schmidt B., Zeeck E. 1999. L-Ovothiol A: The Egg Release Pheromone of the Marine Polychaete *Platynereis dumerilii*: Annelida: Polychaeta // Z. Naturforsch. C. Vol.54. P.1145–1174. DOI: 10.1515/znc-1999-1222

Rotar L.N., Souza J.F. 2019. [Morphological characteristics of the oocyte–cumulus complexes bos taurus and bos indicus of different purpose productivity] // Russ. Agric. Sci. P.64–67 [in Russian, with English summary]. DOI: 10.31857/s2500-26272019364-67

Russo R.I.H. 2014. Techniques and Methodological Approaches in Breast Cancer Research. New York, NY: Springer. XVI, 287 p.

Safieddine A., Coleno E., Salloum S., Imbert A., Traboulsi A.M., Kwon O.S., Lionneton F., Georget V., Robert M.C., Gostan T., Lecellier C.H., Chouaib R., Pichon X., Le Hir H., Zibara K., Mueller F., Walter T., Peter M., Bertrand E. 2021. A choreography of centrosomal mRNAs reveals a conserved localization mechanism involving active polysome transport // Nat. Commun. Vol.12. Art.1352. DOI: 10.1038/s41467-021-21585-7

Sanchez-Arroyo H., Capinera J.L. 2003. House fly, *Musca domestica* Linnaeus // IFAS Ext., Univ. Fla.

Schindelin J., Arganda-Carreras I., Frise E., Kaynig V., Longair M., Pietzsch T., Preibisch S., Rueden C., Saalfeld S., Schmid B., Tinevez J.Y., White D.J., Hartenstein V., Eliceiri K., Tomancak P., Cardona A. 2012. Fiji: an open-source platform for biological-image analysis // Nat. Methods. Vol.9. P.676–682. DOI: 10.1038/nmeth.2019

Schulz K.N., Harrison M.M. 2019. Mechanisms regulating zygotic genome activation // Nat. Rev. Genet. Vol.20. P.221–234. DOI: 10.1038/s41576-018-0087-x

Shirazi A., Sadeghi N. 2007. The effect of ovine oocyte diameter on nuclear maturation // Small Rumin. Res. Vol.69. P.103–107. DOI: 10.1016/j.smallrumres.2005.12.022

Talhouarne G.J., Gall J.G. 2014. Lariat intronic RNAs in the cytoplasm of *Xenopus tropicalis* oocytes // RNA. Vol.20. P.1476–1487. DOI: 10.1261/rna.045781.114

Taylor M.A., Johnson A.D., Smith L.D. 1985. Growing *Xenopus* oocytes have spare translational capacity // Proc. Natl. Acad. Sci. USA. Vol.82. P.6586–6589. DOI: 10.1073/pnas.82.19.6586

Thomas L., Trehin P. 2021. LauLauThom/MaskFromRois-Fiji: Masks from ROIs plugins for Fiji - initial release (1.0.0). // Zenodo. DOI: 10.5281/zenodo.5121890

Valvassori G. 2018. Genomic and phenotypic analyses of polychaete sibling species *Platynereis dumerilii* and *Platynereis massiliensis* in relation to Ocean Acidification. Thesis of Candidate (Ph.D.) of Biological Sci. Degree. Milton Keynes: The Open University. 178 p.

Vastenhouw N.L., Cao W.X., Lipshitz H.D. 2019. The maternal-to-zygotic transition revisited // Development. Vol.146. DOI: 10.1242/dev.161471

Wang L., Stegemann J.P. 2010. Extraction of high quality RNA from polysaccharide matrices using cetyltrimethylammonium bromide // Biomaterials. Vol.31. P.1612–1618. DOI: 10.1016/j.biomaterials.2009.11.024.

Wilson E.B. 1892. The cell-lineage of *Nereis*. A contribution to the cytogeny of the annelid body // J. Morphol. Vol.6. P.361–480. DOI: 10.1002/jmor.1050060301

Winata C.L., Korzh V. 2018. The translational regulation of maternal mRNAs in time and space // FEBS Lett. Vol.592. P.3007–3023. DOI: 10.1002/1873-3468.13183

Responsible editors R.P. Kostyuchenko, E.N. Temereva